Forecasting a Large Number of Tropical Cyclone Intensities around Japan Using a High-Resolution Atmosphere–Ocean Coupled Model

KOSUKE ITO,* TOHRU KURODA, AND KAZUO SAITO

Japan Agency for Marine–Earth Science and Technology, Yokohama, and Meteorological Research Institute, Tsukuba, Japan

AKIYOSHI WADA

Meteorological Research Institute, Tsukuba, Japan

(Manuscript received 15 March 2014, in final form 18 July 2014)

ABSTRACT

This work quantifies the benefits of using a high-resolution atmosphere–ocean coupled model in tropical cyclone (TC) intensity forecasts in the vicinity of Japan. To do so, a large number of high-resolution calculations were performed by running the Japan Meteorological Agency (JMA) nonhydrostatic atmospheric mesoscale model (AMSM) and atmosphere–ocean coupled mesoscale model (CMSM). A total of 281 3-day forecasts were compiled for 34 TCs from April 2009 to September 2012 for each model. The performance of these models is compared with the JMA global atmospheric spectral model (GSM) that is used for the operational TC intensity guidance. The TC intensities are better predicted by CMSM than the other models. The improvement rates in CMSM relative to GSM and AMSM generally increase with increasing forecast time (FT). CMSM is better than GSM and AMSM by 27.4% and 21.3% at FT = 48 h in terms of minimum sea level pressure, respectively. Regarding the maximum wind speed, CMSM is better than GSM and AMSM by 12.8% and 19.5% at FT = 48 h, respectively. This is due to smaller initial intensity errors and sea surface cooling consistent with in situ observations that suppress erroneous TC intensification. Thus, a high-resolution coupled model is promising for TC intensity prediction in the area surrounding Japan, where most of the TCs are in a decay stage. In contrast, coupling to the upper-ocean model yields only a negligible difference in the TC track forecast skill on average.

1. Introduction

Because tropical cyclones (TCs) are often highly destructive, their accurate prediction has been of particular importance in the field of weather forecasting. Track error in forecasts has been almost halved during the past two decades thanks to many improvements in numerical weather prediction systems and observational platforms (National Hurricane Center 2013; Japan Meteorological Agency 2013). Nevertheless, the forecast skill of TC intensity is thought to be a very challenging topic. Because economic damage is related to TC intensity (e.g., Nishijima et al. 2012), improvement in TC intensity forecast skill around Japan is critical for disaster prevention and mitigation of related hazards including strong winds, heavy rainfall, high waves, and storm surges.

Forecasting TC intensities is difficult because the TC intensity depends on finescale inner-core dynamics in addition to interactions with the surrounding synoptic features (Wang and Wu 2004; Emanuel et al. 2004). To reproduce intense TCs explicitly, the horizontal grid spacing in a physics-based model needs to be a few kilometers and nonhydrostatic processes should be taken into account (Yau et al. 2004; Bryan and Rotunno 2009b).

The use of an atmospheric high-resolution model, however, is shown to overestimate TC intensity in some cases (Davis et al. 2008). One possible reason for the overestimation is that storm-induced sea surface cooling is neglected. Atmospheric models usually employ

Denotes Open Access content.

* Current affiliation: University of the Ryukyus, Nishihara, Okinawa, Japan.

Corresponding author address: Kosuke Ito, Dept. of Physics and Earth Sciences, University of the Ryukyus, 1 Sembaru, Nishihara, Okinawa 903-0213, Japan.
E-mail: itokosk@sci.u-ryukyu.ac.jp

DOI: 10.1175/WAF-D-14-00034.1

a virtually constant sea surface temperature (SST) for a lead time of several days. It is an acceptable approximation because oceanic conditions typically change on a time scale of a few months to years. However, this approximation does not hold true near TCs, where SST decreases by 1–6 K on a time scale of several hours to a few days due to shear-induced entrainment at the base of the ocean mixed layer and the oceanic Ekman pumping (e.g., Price 1981; Jacob et al. 2000; Emanuel et al. 2004; Davis et al. 2008; Yablonsky and Ginis 2009; Shay 2010). This cooling leads to a reduction in latent and sensible heat fluxes at the sea surface that suppresses the overintensification of TCs. Previous studies demonstrated that coupled models exhibited better TC intensity forecasting ability in the Atlantic. The Geophysical Fluid Dynamic Laboratory (GFDL) is already equipped with an ocean model coupled to their operational hurricane prediction system for the Atlantic and east Pacific basins. Bender et al. (2007) reported that year-by-year improvements in the GFDL model are partially attributed to the improved reproduction of oceanic features. However, a comparison between the atmospheric model and the coupled model is not provided in their work. Thus, the benefits of coupling to the ocean have not, to date, been isolated based on a large number of samples.

Currently at the Japan Meteorological Agency (JMA), the TC intensity forecasts over the northwestern Pacific including Japan are based on the global atmospheric spectral model (GSM) with a grid spacing of about 20 km. Yu et al. (2013) have already shown that GSM-based guidance has some skill in the prediction of TC intensity. Nevertheless, the ability to forecast intensity can be further improved by using a high-resolution atmosphere–ocean coupled model, as has been done for the Atlantic and east Pacific basins. Although there are several studies on TC–ocean interactions in the northwestern Pacific (Wada 2007; Wada et al. 2010, 2013), the cases are still limited to ascertaining the effects of storm-induced sea surface cooling on TC intensity forecast skill in the vicinity of Japan.

In this study, we conduct a large number of 3-day forecast experiments around Japan in order to obtain a reliable TC intensity forecast assessment. This is achieved by running a JMA nonhydrostatic atmospheric mesoscale model (AMSM) that is similar to an operational regional model and an atmosphere–ocean coupled mesoscale model (CMSM). There are 281 cases that include all the TCs approaching mainland Japan from April 2009 to September 2012 (42 months). This study uses the K computer built in Kobe, Japan, which is a parallel computing system and one of the fastest supercomputers in the world. These intensity forecasts are compared to those obtained from GSM, which is the base model used for JMA operational TC intensity guidance.

This study is the first attempt at isolating the benefits of coupling high-resolution atmospheric models to an ocean model for TC intensity forecasts using a large number of experiments. Comparison with GSM further reveals characteristics of the TC intensity forecasts of high-resolution models. This paper is organized as follows. Section 2 describes the numerical models and the design of the experiments. In section 3, the results of TC-induced sea surface cooling and TC forecasts are evaluated and analyzed. We discuss the model dependency on the initial intensity error and horizontal grid spacing used to define the surface maximum wind speed in section 4. Finally, in section 5, our conclusions are summarized.

2. Experimental design

a. Numerical model

The JMA nonhydrostatic model is used for high-resolution calculations of atmospheric components in this study (Saito et al. 2006; Saito 2012). Model configurations are similar to the JMA operational regional forecast system except that the lateral boundary conditions are coarsely interpolated in this work and forecast time (FT) is extended from 39 h to 3 days [see Japan Meteorological Agency (2014) for details]. This model employs a horizontally explicit and vertically implicit scheme as a dynamical core with six-category bulk microphysics (Ikawa and Saito 1991) and the modified Kain–Fritsch convective scheme. Boundary layer turbulence is solved by the Mellor–Yamada–Nakanishi–Niino level-3 closure model (Nakanishi and Niino 2004) and surface fluxes are calculated by the scheme of Beljaars and Holtslag (1991). The horizontal grid spacing is 5 km on a Lambert conformal projection plane with a vertical representation of 50 layers up to 22 km. The time step is 24 s. We refer to this nonhydrostatic model of the atmosphere as AMSM.

CMSM is very similar to AMSM except that a vertically one-dimensional upper-ocean model developed by Price et al. (1986) is coupled with a grid of the lowest atmospheric layer over the ocean. The diagnostic variables of the upper-ocean model are ocean temperature, salinity, and horizontal components of current velocity. In this model, vertical mixing is calculated by a parameterization scheme satisfying the criteria of density stratification, bulk Richardson number, and gradient Richardson number. Input variables are longwave and shortwave radiation, sensible and latent heat fluxes, and wind stress calculated from the surface wind and drag coefficient. In reality, sea surface stress is affected by ocean coupling due to changes in the wind speed relative

to the sea surface current. However, we do not account for this effect because the wind speed is sufficiently larger than the sea surface current (see Fig. 4, described in greater detail below).

CMSM captures sea surface cooling due to shear-induced vertical mixing referred to as the one-dimensional process in addition to sensible and latent heat exchange. This one-dimensional process follows the local inertial oscillations that have a strong influence on the wake of the storm (Price 1981; Price et al. 1994). In other words, three-dimensional processes such as horizontal advection, Ekman pumping, and inertial-gravity wave propagation are not included. Sea surface cooling is reproduced reasonably well by the one-dimensional process unless the TC translation speed is slower than $5\,m\,s^{-1}$ (Yablonsky and Ginis 2009). The rationale for using the one-dimensional model as a first-order approximation is that the translation speed is usually faster than $5\,m\,s^{-1}$ in this study area (see Fig. 4, described in greater detail below), although sea surface cooling may be underestimated in other cases.

The vertical grid spacing of the upper-ocean model is 5 m. We assume that if the bathymetry H is deeper than 400 m, the bottom depth is set to 400 m in order to save computational time. The upper-ocean model is not coupled if the bathymetry is shallower than 50 m. The bottom temperature and salinity are fixed, and the time step of the upper-ocean model is 10 min. The upper-ocean model provides the updated SST to the atmospheric model every 10 min for a given surface wind vector, drag coefficient, and surface heat flux, including longwave and shortwave radiation. The simple physics, configuration, and long time step of the upper-ocean model increase the computational time only by about 1% relative to the original AMSM.

The results of AMSM and CMSM are compared to the TC intensity forecasts based on GSM preserved in file storage at JMA. GSM employs primitive equations and incorporates the Arakawa–Schubert scheme and the Mellor–Yamada level-2 closure scheme. In the horizontal coordinate, prognostic variables are spectrally discretized using triangular truncation at wavenumber T959. The corresponding transform grids cover about 0.1875° in both latitude and longitude (approximately 20 km). In the vertical grid, the model has 60 layers up to 0.1 hPa. Note that we compare the results to the GSM output and not to the GSM-based guidance.

b. Initial and boundary conditions

The initial states of AMSM and CMSM are provided by the JMA nonhydrostatic model–based variational data assimilation system (JNoVA; Honda and Sawada 2009), while the initial states of the GSM are given by the GSM-based variational data assimilation system (Japan Meteorological Agency 2014). TC bogus data are ingested as observations in these data assimilation systems. Lateral boundary conditions of AMSM and CMSM are given by the GSM forecast interpolated on 16 pressure levels at a time interval of 6 h. This approach is different from the JMA operational regional forecast system that uses 50 model levels at a time interval of 1 h as the lateral boundary conditions. The initial SSTs in GSM, AMSM, and CMSM are obtained from the Merged Satellite and In-situ Data Global Daily SST (MGDSST) used by JMA (Kurihara et al. 2006; Japan Meteorological Agency 2014). SSTs during the forecast period in AMSM and GSM are unchanged (except for a very small seasonal change in GSM based on the climatology). In contrast, the SST in CMSM is dynamically changed as a response to atmospheric forcing.

We construct the initial oceanic state in CMSM as follows. First, we calculate the daily climatology obtained from the monthly mean climatology data of temperature and salinity in the *World Ocean Atlas 2009* (Locarnini et al. 2010; Antonov et al. 2010) by linearly interpolating the climatology in time onto a day of the month. Then, we define the mixed layer as a layer with a density difference of less than $0.125\,kg\,m^{-3}$ from the surface. That SST anomaly with respect to the daily climatology is assumed to be the same as the temperature anomaly within the mixed layer. The initial ocean temperature beneath the ocean mixed layer and the ocean salinity are set to the daily climatology, although recent studies have reported that the subsurface oceanic state has a large impact on TC intensity (Lin et al. 2005, 2008; Yablonsky and Ginis 2009; Shay 2010; Lloyd and Vecchi 2011). The initial ocean current is considered to be at rest for simplicity. We perform a forecast experiment with this simple setting as a first step toward clarifying the contribution from ocean coupling.

In this setting, some imbalances are introduced at the initial time due to ocean temperature anomalies within the mixed layer and the use of a one-dimensional model that cannot achieve geostrophic balance. These imbalances do not incur the notable initial shock in the current experiment. However, they should be corrected in future works by employing a three-dimensional ocean model with a more realistic ocean reanalysis dataset for the initial conditions.

c. Verification

The calculation domain is the same as that used in the JMA operational regional forecast as of 2012. The domain has 721×577 grid points with a grid spacing of 5 km and includes Japan and its surrounding areas

(Fig. 1; http://www.jma.go.jp/jma/jma-eng/jma-center/nwp/specifications_models.pdf).[1] We regard the calculation domain, excluding the region within 500 km from the lateral boundary, as a verification region (Fig. 1). Figures 2a and 2b indicate the estimated mean dynamic topography above the geoid and the exemplar sea surface height anomalies, respectively, during September 2010 with respect to a 20-yr mean profile (1993–2012), which is obtained from Archiving, Validation, and Interpretation of Satellite Oceanographic data (AVISO). It shows that the Kuroshio passes south of Japan and that there are some warm and cold eddies in the southeast part of the study area, particularly around the Kuroshio Extension region.

We conduct 3-day forecast experiments by running AMSM and CMSM four times a day at 0000, 0600, 1200, and 1800 UTC for all of the TCs from April 2009 to September 2012 (42 months) when the TC center position is located in the verification region according to the Regional Specialized Meteorological Center Tokyo best track (hereafter referred to as RSMC best track).

There is no consensus on the best method for comparing a wind speed obtained from numerical models with the maximum speed of an actual 10-min sustained surface (10-m height) wind in reality. This lack of consensus is due to disagreement over the model representation: the horizontal grid spacing (Walsh et al. 2007); the time representativeness, including the temporal period for calculating an average; and the use of physical parameterization such as a cloud parameterization scheme or a bulk scheme for a surface boundary layer model that represents a time-mean state. To define surface maximum wind speed V_{max} in AMSM and CMSM for comparison with GSM, we use a snapshot maximum of the 4×4 gridbox mean (20 km $\times$ 20 km). We obtain the 10-m height wind speed by applying dimensionless stability functions to the wind speed at the atmospheric lowest model layer (20-m height). The dependency of TC intensity on the horizontal gridbox size is investigated in section 4b.

We regard the storms in AMSM and CMSM as TCs if the threshold of 850-hPa wind velocity exceeds 21.5 m s^{-1}, which roughly corresponds to 17.2 m s^{-1} at the surface (Franklin et al. 2003). To exclude midlatitude extratropical cyclones, we also use the structural requirement that a sum of the temperature deviations at 300, 500, and 700 hPa above the center exceeds 2 K, as in Oouchi et al. (2006). This ensures that the storms have a warm core.

[1] In March 2013, the domain in the JMA operational regional forecast was extended to 817 $\times$ 661 grid points.

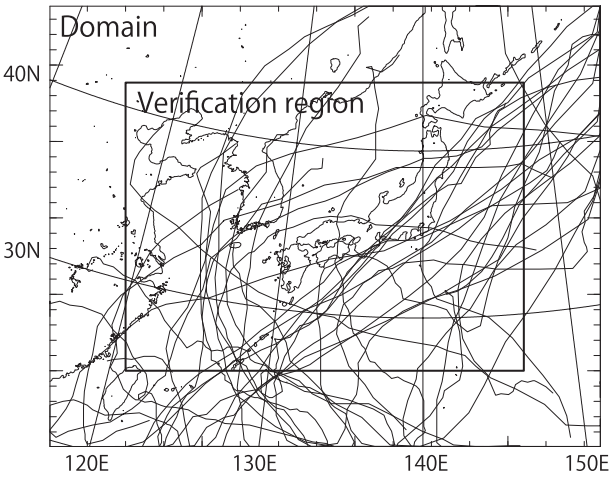

FIG. 1. The domain used in this experiment. The thick box indicates the verification region. The thin lines indicate TC positions from RSMC best track that are used in this study.

To trace the translating TCs in AMSM and CMSM, we use criteria similar to those used by the Working Group on Numerical Experimentation (WGNE), jointly established by the World Climate Research Programme (WCRP) Joint Scientific Committee (JSC) and the World Meteorological Organization (WMO) Commission for Atmospheric Sciences (CAS), Intercomparison of TC Track Forecasts (Sakai and Yamaguchi 2005). The TC position error is defined as an absolute distance between the RSMC best track and the corresponding predicted TC position. The predicted TC position is defined as the location of the minimum sea level pressure P_{min} at 6-h intervals within 500 km from the guess point. The guess point for each FT is determined as follows: 1) Initial time and FT = 6 h, the RSMC best track position; and 2) FT = 12 h or later, a linearly extrapolated position from the last two forecast positions. The guess point is used to avoid falsely detecting the local P_{min} point away from the presumable storm as the TC center. In the case that there are no P_{min} points satisfying the criteria of a TC, the tracking is terminated. Forecast skill is not evaluated if there is a TC in the numerical model without the corresponding best-track data, and vice versa.

The total numbers of TCs and forecast experiments are 34 and 281, respectively. Corresponding TC trajectories in the RSMC best track are plotted in Fig. 1. Table 1 indicates that the numbers of cases during each forecast time are very similar among GSM, AMSM, and CMSM for the same verification time. This is partly because TC track prediction is not substantially influenced by the use of the high-resolution model and the coupling with the upper-ocean model as shown in section 3c. Figure 3 provides the average and standard

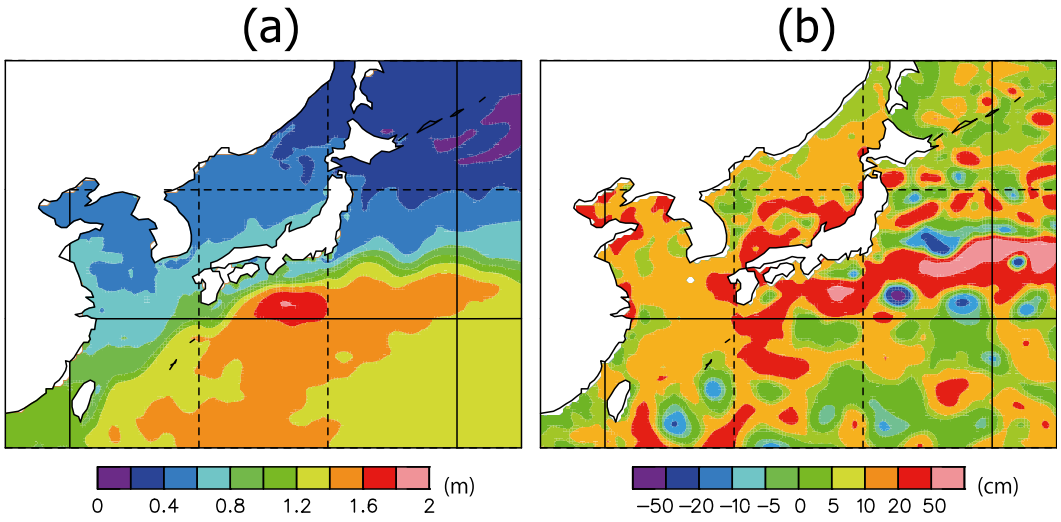

FIG. 2. (a) Estimate of the ocean mean dynamic topography (m; MDT_CNES-CLS09_v1.1) and (b) exemplary monthly mean map of the sea level anomaly (cm) during September 2010 from AVISO. MDT_CNES-CLS09 was produced by the Collecte Localisation Satellites (CLS) Space–Oceanography Division and distributed by AVISO, with support from the Centre National d'Études Spatiales (CNES; http://www.aviso.oceanobs.com/). The altimeter products were produced by Segment Sol multimissions d'ALTimétrie, d'Orbitographie et de localisation précise/Data Unification and Altimeter Combination System (SSALTO/DUACS) and distributed by AVISO, with support from CNES (http://www.aviso.altimetry.fr/duacs/).

deviations of P_{min} of the TCs used in this study based on the RSMC best track. Figure 3 shows that the TCs tend to decay and standard deviations of the TC intensities shrink with increasing forecast time for the study area.

3. Results

a. Oceanic state

First, an oceanic response to TC-related wind forcing in CMSM is briefly summarized to validate the quality of the ocean coupling. Figure 4 shows a composite of the SST changes at FT = 36 h (relative to the initial SST at the same geographical point). In Fig. 4, the coordinate represents the along- and cross-track distances centered at the TC position at FT = 36 h, in which a direction of TC motion is determined by the difference between the TC positions at FT = 30 and 36 h. The results are classified into three groups according to the TC translation

TABLE 1. Number of cases used in the verification.

FT (h)	GSM	AMSM	CMSM
0	281	281	281
6	252	248	248
12	221	217	217
18	193	189	190
24	164	161	160
30	139	139	138
36	118	117	117
42	95	96	95
48	79	76	75
54	63	60	59
60	47	45	45
66	36	34	34
72	28	26	25

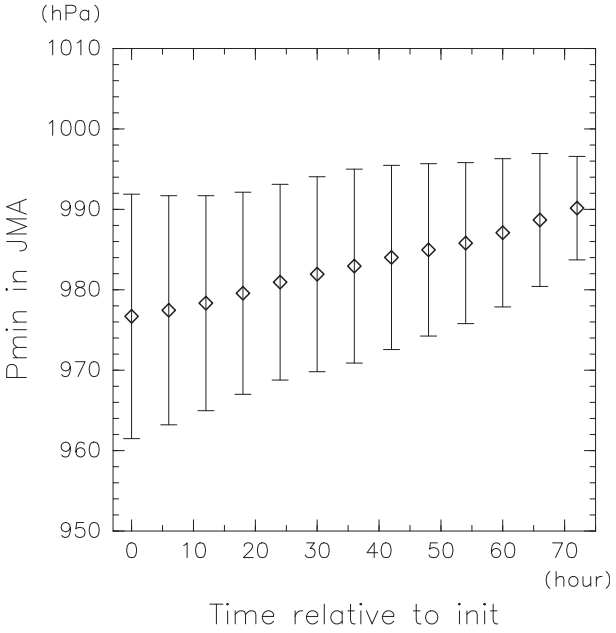

FIG. 3. Composite mean of P_{min} at each verification time with its std dev (hPa) according to the RSMC best track used in this study.

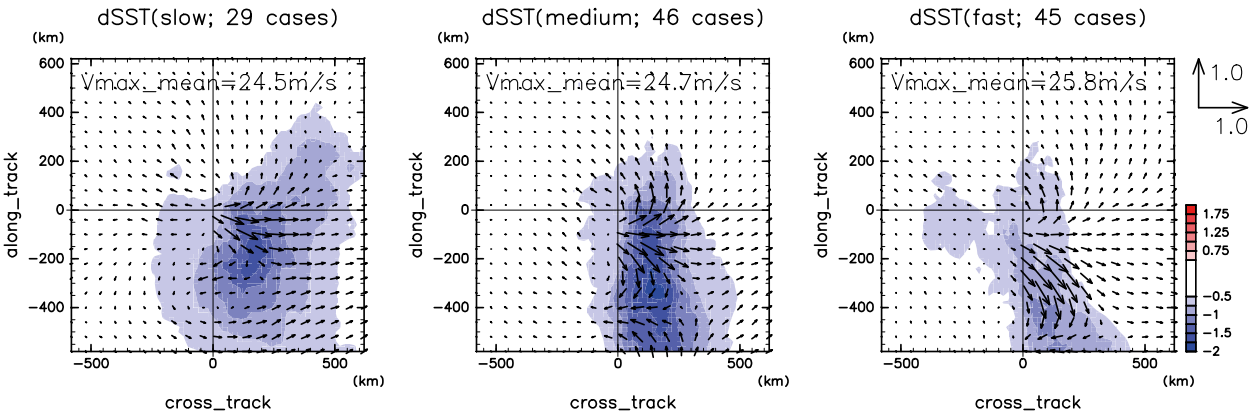

FIG. 4. Sea surface cooling (K; shading) at FT = 36 h (relative to the initial time) in the storm-centered coordinate classified into three groups according to the TC translation speed: (left) slow (<5 m s^{-1}), (middle) medium (5–9 m s^{-1}), and (right) fast (>9 m s^{-1}). Horizontal components of the surface current (m s^{-1}) are overplotted in the vector. Unit vector is given (right) and values are the averages of V_{max} in each group.

speed: slow (<5 m s^{-1}), medium (5–9 m s^{-1}), and fast (>9 m s^{-1}) cases.

Figure 4 shows that sea surface cooling is maximized in the right-rear quadrant. As the TC translation speed increases, the location of the maximum cooling moves away from the center. The magnitudes of the maximum sea surface cooling are 1.6, 1.8, and 1.1 K in the slow-, medium-, and fast-translating TCs, respectively. These results indicate that the slow-translating TCs do not produce the largest cooling. One possible reason for this is that there is a difference in the underlying oceanic conditions. Figure 5 displays the ocean temperature beneath the TC position at FT = 0 h averaged over the region within 500 km from the TC center position at FT = 36 h. Initial ocean temperature decreases rapidly in the vertical direction (0–20 m) beneath TCs translating at medium and fast speeds, which contributes to larger sea surface cooling.

A composite of horizontal current at the surface calculated from the upper-ocean model is plotted in Fig. 4. The upper-ocean model used in this study "locally" (i.e., no interaction with horizontally adjacent grids) calculates the horizontal current rotating in a clockwise direction due to the inertial oscillations. Because the wind stress vector also rotates clockwise on the right-hand side of the TC pathway, the vector is roughly resonant with the current velocity in the right-rear quadrant (Price 1981). The resultant strong current causes a relatively deep mixing and marked sea surface cooling (Price 1981; Price et al. 1994). These features are consistent with previous studies that have described the oceanic responses to TC-like wind forcing (e.g., Price 1983; Ginis and Sutyrin 1995; Jacob et al. 2000; Lin et al. 2005, 2008; Yablonsky and Ginis 2009).

To validate the quality of the coupled model further, we compare the SST to in situ observations. We derive Argo float–based SST, or SST_{Argo}, by vertically averaging ocean temperature from the surface to 10-m depth. These data are compared with the corresponding model output at the same location and time. A float is employed for validation if the Argo float is located within 500 km (1000 km) from the TC center in the RSMC best track. We used the dataset known as delayed mode data, which

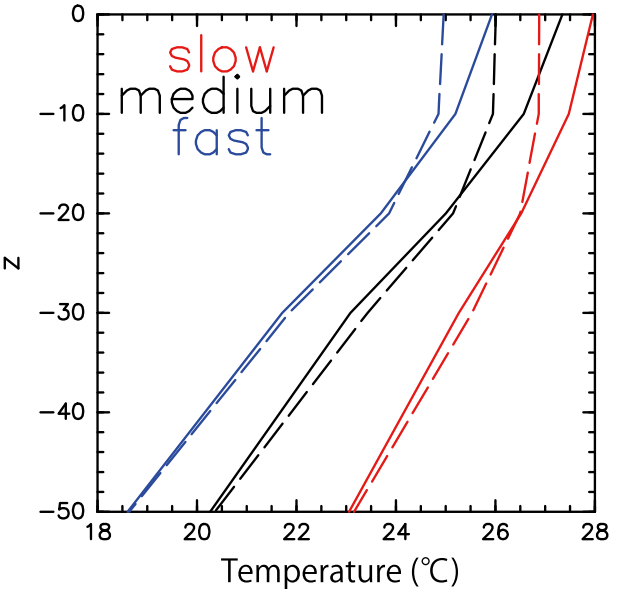

FIG. 5. Ocean temperature profile (°C) at FT = 0 (solid lines) and 36 h (broken lines) averaged over the region within 500 km from TC center position at FT = 36 h for the slow- (red), medium- (black), and fast-translating (blue) TCs. Vertical axis is the depth (m).

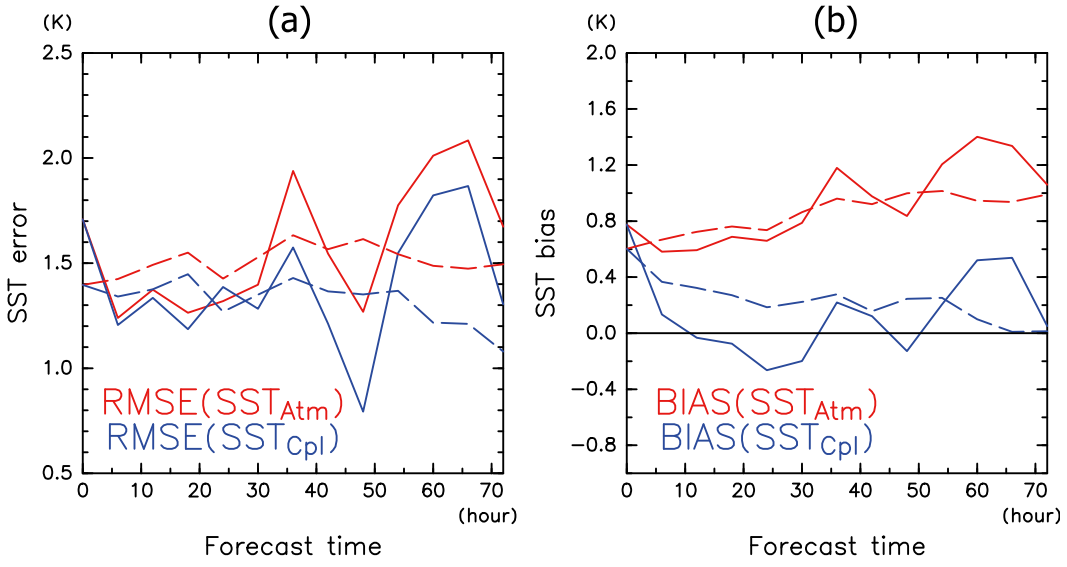

FIG. 6. (a) RMSE of the SST used in the atmospheric model (red) and coupled model (blue) relative to Argo floats. Solid (broken) lines indicate the RMSE against the Argo floats within a distance of 500 (1000) km from the TC center position in the RSMC best track. (b) As in (a), but for mean bias of SST.

had already been subject to sufficient quality control. This dataset is compared to SSTs obtained from the coupled (Cpl) model (CMSM) SST_{Cpl} and SSTs originally used in the atmospheric (Atm) models GSM and AMSM SST_{Atm}. The number of available floats within 500 km (1000 km) is 36 (145) at FT = 24 h, 18 (68) at FT = 48 h, and 12 (44) at FT = 72 h. Here, the depth-averaged ocean temperature in Argo floats was compared with the SST in CMSM instead of the depth-averaged (from surface to 10-m depth) ocean temperature in CMSM. This difference caused only a negligible change in the root-mean-square error (RMSE) and a mean bias in the SST of less than 0.1 K throughout the forecast time. Please remember that there is no spinup run for initializing the oceanic state in CMSM. Therefore, the difference between AMSM and CMSM purely reflects the sea surface cooling at the forecast time.

Figure 6a shows the RMSEs in SST_{Atm} and SST_{Cpl}, where an Argo float is deployed. The RMSEs in SST_{Cpl} are smaller than those in SST_{Atm}. In particular, the CMSM-derived SST is more consistent with in situ observations with increasing forecast time. The RMSEs in SST_{Cpl} are smaller by about 40% at FT = 72 h in comparison with those in SST_{Atm}.

The difference in RMSE between SST_{Atm} and SST_{Cpl} is partly explained by a positive SST bias. Figure 6b shows the composite mean bias in SST_{Atm} and SST_{Cpl} with respect to SST_{Argo}. A positive bias of 0.6 K is found at the initial time. The positive SST bias at the initial time may be due to signals with a period of shorter than 27 days that are cut off in MGDSST in order to diminish noise in this range (Japan Meteorological Agency 2014). This omission may reduce the signature of the sea surface cooling associated with the TC passage. The positive bias increases from 0.6 to 1.0 K in SST_{Atm} with increasing forecast time. On the other hand, the mean bias of SST_{Cpl} is considerably closer to 0 K, suggesting that the upper-ocean model reasonably reproduces the mean sea surface cooling during the TC passage. Hence, the TC intensity in CMSM is expected to be closer to that of the corresponding best track, as is demonstrated in the next subsection.

b. TC intensity

Figure 7a shows the RMSEs in P_{min} for GSM, AMSM, and CMSM relative to the RSMC best track. CMSM generally exhibits the best forecast skill among the three, and the high-resolution models (AMSM and CMSM) are better than GSM throughout the forecast time. The difference between AMSM and CMSM is noticeable at FT = 36 h and later. The rates of improvement in CMSM relative to GSM (AMSM) are 10.9% (3.4%) at FT = 24 h, 27.4% (21.3%) at FT = 48 h, and 40.5% (28.9%) at FT = 72 h. RMSEs in AMSM and GSM steadily increase with increasing forecast time, while RMSE in CMSM tends to saturate.

Figure 7b shows that the RMSE in V_{max} is generally the smallest in CMSM throughout the forecast time. The initial error is much smaller in the high-resolution models. The forecast skill of GSM improves more than that of AMSM after FT = 24 h. The RMSE in AMSM increases with increasing forecast time, while those in GSM and

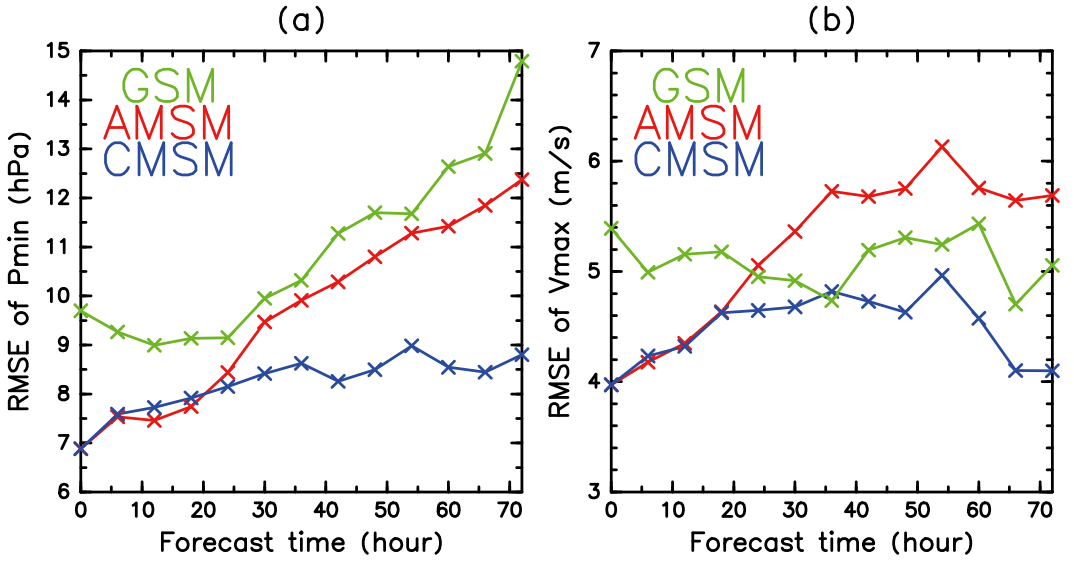

FIG. 7. RMSE of (a) P_{min} and (b) V_{max} relative to the RSMC best track. The results are shown for GSM (green), AMSM (red), and CMSM (blue).

CMSM do not. The rates of improvement in CMSM relative to GSM (AMSM) are 6.2% (8.1%) at FT = 24 h, 12.8% (19.5%) at FT = 48 h, and 18.9% (27.9%) at FT = 72 h. The RMSE in AMSM steadily increases with increasing forecast time, while that in CMSM tends to saturate or even decrease during the later period of the forecast time.

Generally, Fig. 7 indicates that CMSM outperforms GSM and AMSM in the forecasting ability of both P_{min} and V_{max}. Because RMSE is the square root of the sum of the squared mean bias and residual, we proceed to investigate the mean biases in GSM, AMSM, and CMSM. Figure 8 shows the mean biases of P_{min} and V_{max}. TCs are weakly reproduced at the initial time in all of the models although this situation is slightly improved in AMSM and CMSM on average. This is because a better initial value that is generated by the high-resolution model-based data assimilation system, JNoVA, is used in AMSM and CMSM.

Figure 9 shows scatterplots for P_{min} and V_{max} at the initial time for both the models and the best track. The intensities of strong TCs are not well reproduced in GSM at the initial time. The reproduction is improved in the high-resolution models (AMSM and CMSM). The

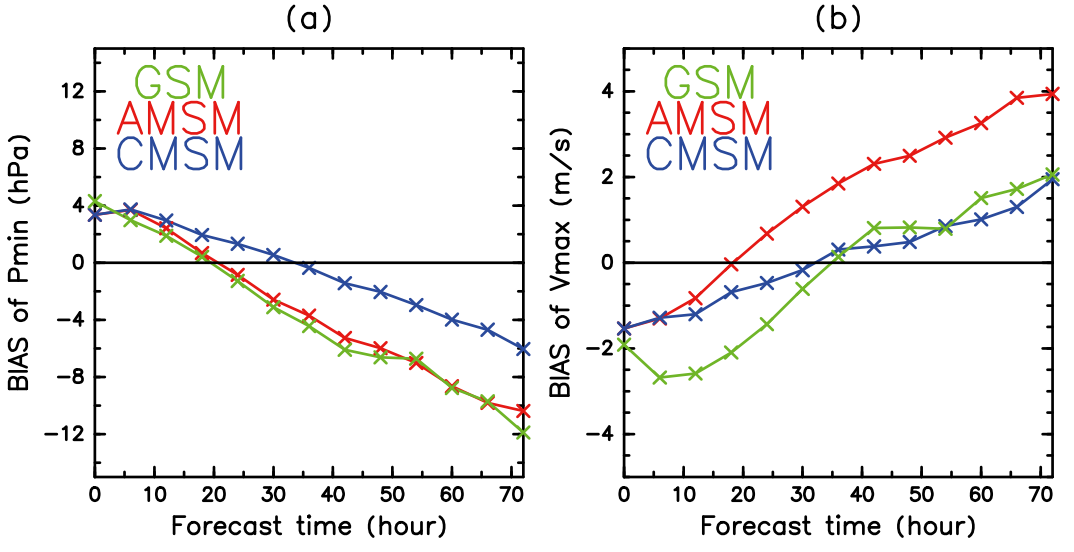

FIG. 8. Composite mean bias for (a) P_{min} and (b) V_{max} in each forecast time.

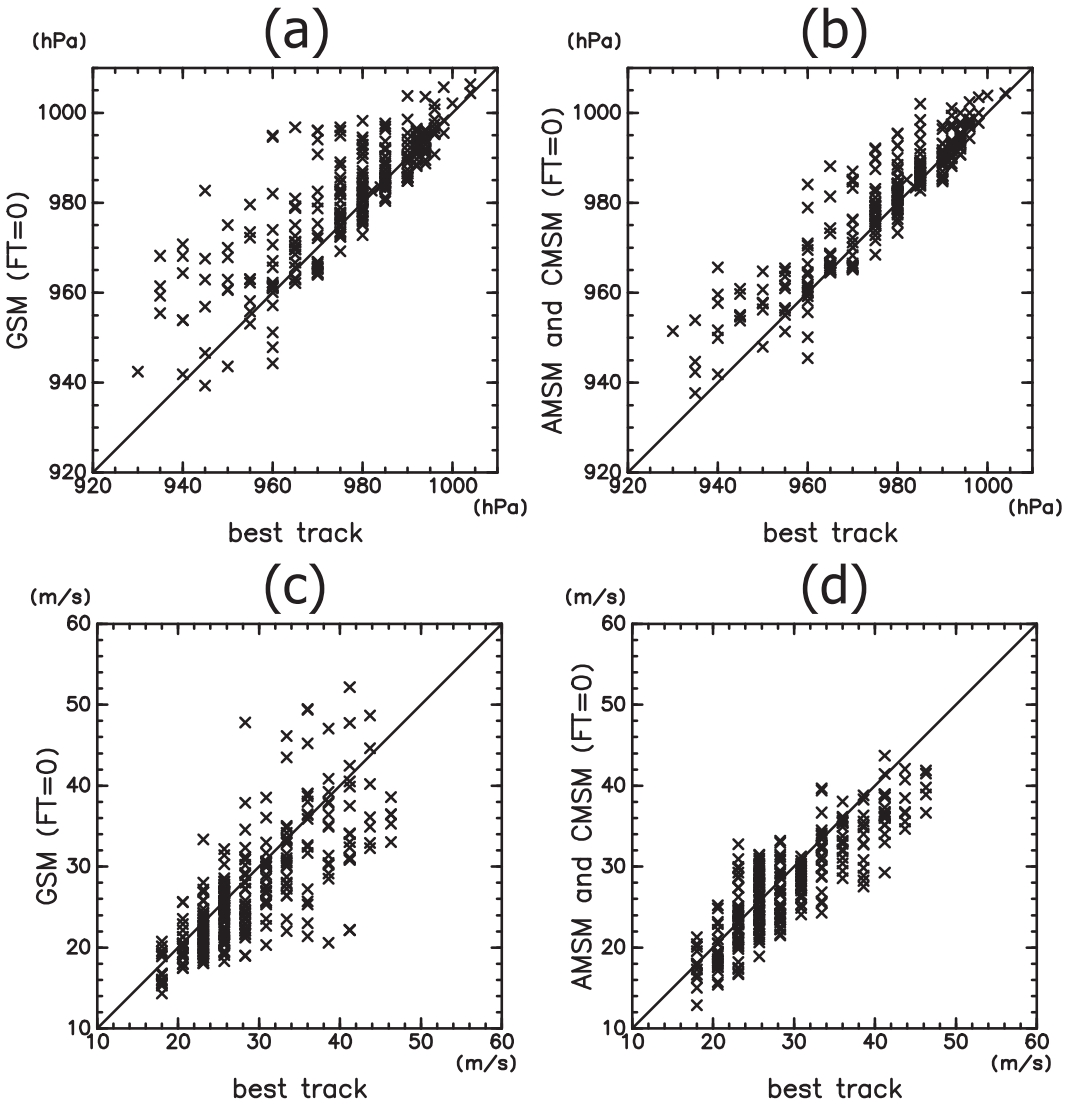

FIG. 9. (a),(b) Scatterplot of P_{min} at FT = 0 h. The marks indicate the P_{min} of the RSMC best track and the corresponding model output in GSM (a) and high-resolution models (AMSM and CMSM) (b). (c),(d) As in (a),(b), but for V_{max}.

initial mean bias of P_{min} is 10.3 hPa in GSM (6.4 hPa in AMSM and CMSM) for the strong TCs ($P_{min} <$ 970 hPa), while it is 2.2 hPa in both GSM and the high-resolution models for the weak TCs ($P_{min} >$ 970 hPa). This indicates that P_{min} of weak TCs is slightly high in all the models at the initial time, while P_{min} of strong TCs is better reproduced in the high-resolution models. As for V_{max}, the initial mean bias is $-3.5\,m\,s^{-1}$ in GSM ($-3.8\,m\,s^{-1}$ in AMSM and CMSM) for strong TCs ($P_{min} <$ 970 hPa), while it is $-1.2\,m\,s^{-1}$ ($-0.8\,m\,s^{-1}$ in AMSM and CMSM) for the weak TCs ($P_{min} >$ 970 hPa). However, as indicated in Fig. 9c, the correlation coefficient between V_{max} in the model and the corresponding value in the best track is as low as 0.27 in GSM for the intense TCs, while it is 0.66 in AMSM and CMSM. These facts reveal that the TC intensity is more consistent with the high-resolution models.

In the later period of the forecast, P_{min} becomes too low, particularly in the noncoupled models (Fig. 8a). The mean bias is 6 hPa at FT = 48 h and 10–12 hPa at FT = 72 h. Figure 8b shows that V_{max} is too strong in AMSM, while the mean bias is relatively small in CMSM. This overintensification in the later period of the forecast is highly suppressed in CMSM accompanied by sea surface cooling. The mean bias of P_{min} (V_{max}), on average, decreases by about 4 hPa ($2\,m\,s^{-1}$) at FT = 48 h and 6 hPa ($2\,m\,s^{-1}$) at FT = 72 h relative to AMSM. This substantially improves the TC intensity forecast skill of CMSM. At FT = 36 h,

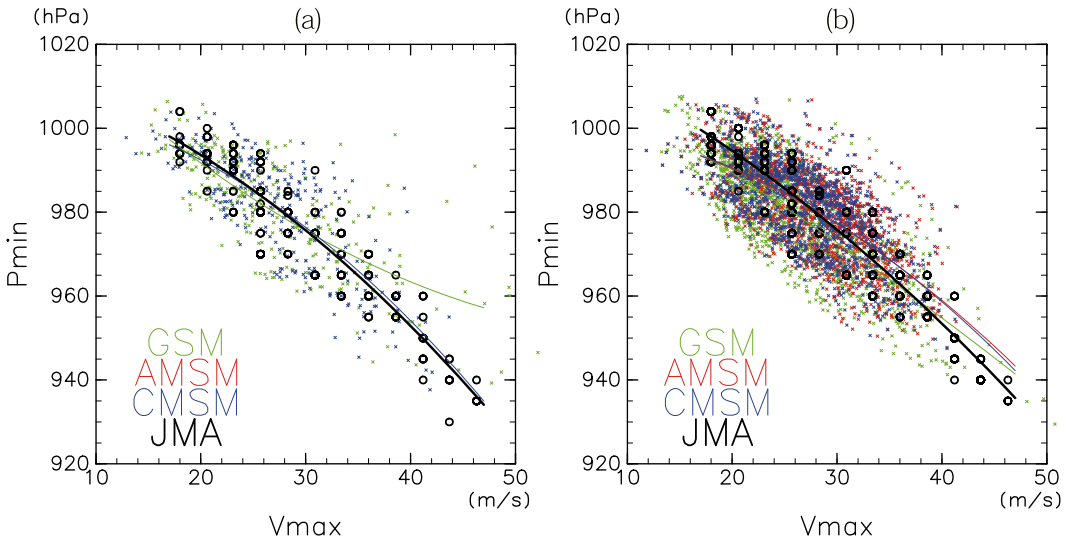

FIG. 10. Scatter diagram of V_{max} (m s^{-1}) and corresponding P_{min} (hPa) in GSM (green), AMSM (red), CMSM (blue), and the RSMC best track (black) for (a) FT = 0 and (b) FT > 0 h. Solid lines of the corresponding colors show the second-order polynomial fit to the data points. Note that the initial conditions in AMSM are the same as in CMSM.

GSM exhibits better skill for V_{max} determination in terms of RMSE than CMSM does. This is partly because the mean bias is nearly zero in GSM as it turns into a positive bias. Here, we do not show the details of the residual term, but the residual term of RMSE is the smallest in CMSM for most of the forecast time, for both P_{min} and V_{max} (figures not shown).

It is interesting that GSM exhibits comparable or better skill than AMSM during the later period. This result can be explained by the magnitude of overintensification. A fine-mesh calculation usually yields more intense TCs by resolving the inner-core structure that may lead to the severe overintensification of the storm in AMSM relative to GSM (Fig. 8). This implies that the use of high-resolution models without coupling to an ocean model may degrade the TC intensity forecast skill. Meanwhile, overintensification in the high-resolution model is much suppressed by sea surface cooling following the realistic reproduction of SST.

In summary, although TCs are weakly reproduced initially, their reproduction is improved in the high-resolution models for strong TCs. TCs tend to become overintensified with increasing forecast time if the model is not coupled with an ocean model. Sea surface cooling in CMSM suppresses the unrealistic intensification of TCs and contributes to more realistic TC intensity prediction. The benefits of high-resolution coupled models are very robust in terms of TC intensity forecasts based on a large number of samples.

It is interesting that the RMSEs in CMSM show a saturating or decreasing trend for P_{min} and V_{max} with increasing forecast time. One reason for this trend is that the variability in TC intensity tends to shrink (Fig. 3). Because the mean bias is kept small in CMSM, RMSE is also kept nearly constant. In contrast, the error in TC intensity forecast with AMSM grows along with the increasing mean bias during the later period of the forecast.

To further assess the quality of the TC intensity forecasts, the relationship of pressure–wind speed at FT = 0 h is displayed in Fig. 10a for GSM, AMSM, CMSM, and the RSMC best track. The solid lines indicate the second-order polynomial fit to the data points. For the intense TCs, P_{min} in GSM is much higher than that in the best track for a given V_{max}. These cases are mostly seen in the 2009 data. This may be attributed to the old JMA bogus scheme used until October 2009 that had introduced a steep horizontal gradient and caused an unrealistic deformation of the initial fields for some TCs (Kosaka and Okagaki 2010). In contrast, the initial TC P_{min}–V_{max} relationship is represented accurately in the high-resolution models. Excluding FT = 0 h, the relationship is reasonably captured by all the models (Fig. 10b). On closer inspection, P_{min} in the numerical models is likely to be slightly high (low) for a given V_{max} for strong (weak) TCs. This is in contrast to previous studies. For example, Manganello et al. (2012) used a grid spacing of 10 km that showed that P_{min} is slightly low for a given V_{max} for strong TCs.

We stratify the results of the P_{min} forecast at FT = 48 h into five groups according to the intensity change in the best-track data that is defined as the difference in P_{min} between FT = 24 and 48 h in order to check the dependency (Table 2). As previously observed, most

TABLE 2. RMSEs of P_{min} at FT = 48 h stratified according to the intensity change.

	GSM			AMSM			CMSM		
$P_{48\,h} - P_{24\,h}$	RMSE (hPa)	Bias (hPa)	Case	RMSE (hPa)	Bias (hPa)	Case	RMSE (hPa)	Bias (hPa)	Case
<0	7.8	2.6	7	8.4	3.7	6	11.9	9.2	6
0–5	11.1	−6.9	26	12.9	−9.3	26	8.8	3.9	26
5–10	11.9	−6.8	15	11.5	−5.8	13	9.6	−2.8	13
10–15	15.6	−11.5	12	11.2	−6.6	12	8.5	−2.9	12
>15	10.6	−6.5	19	6.9	−4.2	19	5.2	1.9	18

TCs are decaying in this region. The bias in CMSM is smaller than that in GSM and AMSM regardless of the rate of decay. This indicates that the coupling with the ocean model improves the decaying TC intensity prediction. Nevertheless, TC intensity in a developing stage is not predicted well, particularly in CMSM, although the number of cases is small. These include one case for Typhoon Talas (2011), four cases for Damrey (2012), and one to two cases for Haikui (2012). As for Talas, in which the intensity bias is the largest, a TC in all models makes its landfall too early (figures not shown). This leads to unrealistically weak TCs at the verification time in the numerical models. In the other cases, the TC track and initial TC intensity are reproduced reasonably well. One possible explanation is that the intensity of developing TCs is not fully reproduced without using a horizontal grid spacing of less than 2 km (Davis et al. 2008). However, the detailed analysis of this possibility is left for future work.

c. *Track forecast skill*

While the main scope of the current work is TC intensity forecasts, it is worth investigating the impact of the high-resolution model and ocean coupling on the TC track forecast skill based on large samples. If the track forecasts vary significantly, TC intensity is also influenced by changes in environmental conditions. Figure 11 represents the TC track forecast skill. Here, GSM is better than AMSM and CMSM. AMSM is better than CMSM, although the difference is not large. This is partly because the initial TC position is more consistent with the best track in GSM. Another possible reason is that the lateral boundary conditions in AMSM and CMSM are coarsely interpolated in time in this study so that the forecast of large-scale flow pattern is degenerated.[2]

Figure 12 shows TC center positions at FT = 36 h for each experiment in AMSM, CMSM, and GSM relative to the RSMC best track. The data are stratified in the along- and cross-track coordinates, as in Fig. 4. This shows that AMSM and CMSM have positive biases in the along-track direction, while a negative bias is found in GSM. On closer inspection, the mean TC positions in CMSM are located slightly to the left (about 14 km) of the storm motion in comparison with that in AMSM. This implies that the ocean coupling slightly deflects the TC position to the left because sea surface cooling on the right-hand side is not favorable for the storm. Although this difference tends to increase when increasing the forecast time, the mean TC position difference between AMSM and CMSM is less than 20 km throughout the forecast period (figures not shown). In some cases, the position differences among GSM, AMSM, and CMSM are a few hundred kilometers. However, the large-scale environmental factors that affect the TC intensity are not expected to be very different in many cases.

4. Discussion

a. *Dependency on initial error*

To further improve TC intensity forecast quality, the use of finer grid resolution and more sophisticated physical schemes that include better representations of the initial TC intensity and initial environmental conditions are recommended. Among these, we can estimate the contribution of the initial TC intensity error from the current set of experiments. Figures 13a–c show the relationships between the initial P_{min} error and the P_{min} error at FT = 24, 48, and 72 h in CMSM, respectively. Figures 13d–f are similar to Figs. 13a–c, but for the V_{max} error.

TC intensity forecast skill is dependent on the TC intensity error at the initial time, particularly for a forecast of less than 2 days. Based on a significant Student's t test, the confidence levels for the correlation coefficients between the initial errors and the errors of P_{min} (V_{max}) at FT = 24, 48, and 72 h are >99.99% (>99.99%), 99.00% (99.98%), and 96.18% (95.03%), respectively. This implies that a better representation of the initial TC

[2] In 2003, the Numerical Prediction Division of JMA confirmed that model performance was degenerated with increasing time interval from 1 h for its boundary condition update (J. Ishida 2013, personal communication).

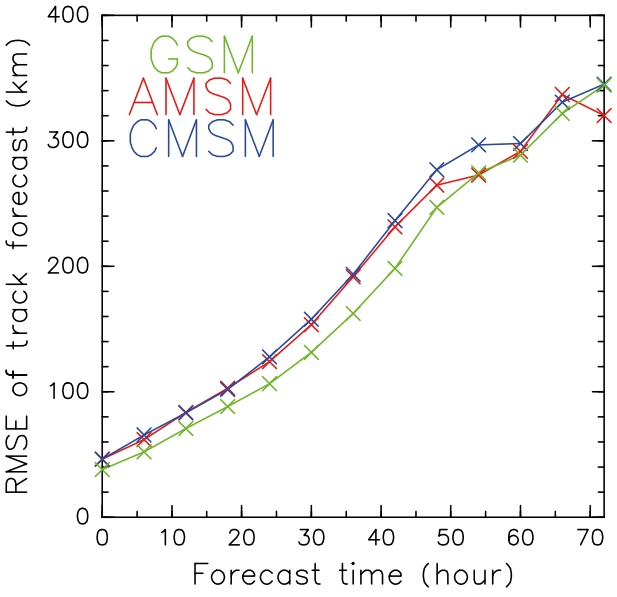

FIG. 11. As in Fig. 7, but for the TC track forecast.

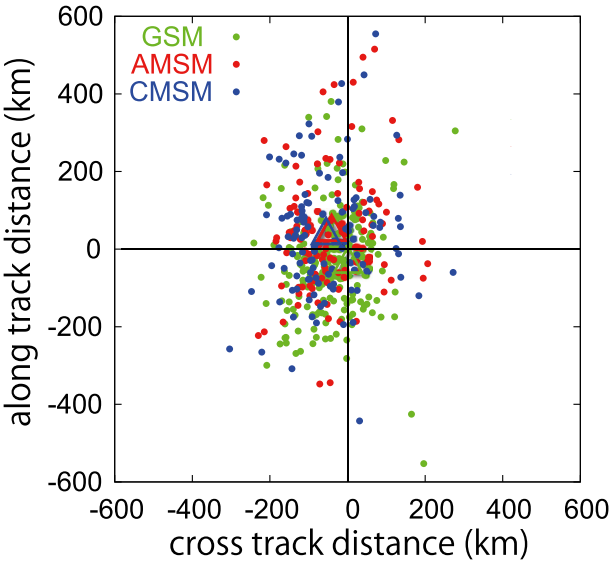

FIG. 12. TC center position at FT = 36 h for each experiment in GSM (green), AMSM (red), and CMSM (blue) relative to the RSMC best track. Vertical axis is the along-track distance in the direction of the model TC motion from FT of 30 to 36 h, while the horizontal axis is the cross-track distance. Triangles indicate the mean position bias in the same color.

intensity contributes to improvement of the TC intensity forecasts in addition to the use of fine-mesh, improved determination of initial environmental conditions, and model physics. A better initial TC intensity can be obtained from the use of fine-mesh, improved bogussing techniques, and enhanced specification of air–sea exchange coefficients in the data assimilation system (Ito et al. 2010, 2013).

b. *Dependency on the gridbox size*

As mentioned previously, 4 × 4 gridbox (20 km × 20 km) averaged values in AMSM and CMSM are used to define V_{max} for a fair comparison with GSM in this study. Here, we investigate the dependency of the forecast skill on the gridbox size in AMSM and CMSM: 1 × 1, 2 × 2, 4 × 4, and 8 × 8 (Fig. 14a).

Figure 14 shows that CMSM exhibits the best forecast skill of V_{max} regardless of the choice of the gridbox size, although there are some differences in the RMSE of V_{max}. Thus, V_{max} is not very sensitive to the gridbox size. Differences among the different gridbox sizes can be explained by the differences in the mean bias (Fig. 14b). The mean bias of V_{max} decreases by 1 m s^{-1} between the 1 × 1 gridpoint value and the 8 × 8 gridbox-averaged value. The smaller RMSEs using an 8 × 8 gridbox in the later period are relevant to the smaller mean bias.

5. Summary

To improve TC intensity forecasts, a high-resolution atmosphere–ocean coupled model is promising because it can represent the inner-core dynamics and sea surface cooling associated with a storm's passage. In this work, we conduct a set of 281 3-day forecast experiments around Japan by using the JMA nonhydrostatic atmospheric mesoscale model (AMSM) and AMSM coupled with a simple upper-ocean model (CMSM) to quantify the benefits of a high-resolution atmosphere–ocean coupled model by using large parallel computing resources. The calculation domain is the same as that used in the JMA operational regional forecast as of 2012 and most TCs are in a decay stage. This study covers all of the 34 TCs that passed through the verification region from April 2009 to September 2012. The results are compared to those obtained from using the global atmospheric spectral model (GSM), which is the base model of the operational TC intensity guidance. The horizontal grid spacing is 5 km in the high-resolution models (AMSM and CMSM) and about 20 km in GSM.

The one-dimensional upper-ocean model used in CMSM can address the vertical mixing alongside the surface current divergence in the right-rear quadrant of the TC position. We assume that the anomaly of the initial ocean temperature in the mixed layer is the same as that of SST and that the remaining oceanic conditions follow the climatology. Even though the configuration of the ocean is quite simple, the resultant sea surface cooling is consistent with previous studies. The mean bias of SST in CMSM is nearly zero with respect to the Argo floats on average. In contrast, the original SSTs used in AMSM and GSM are

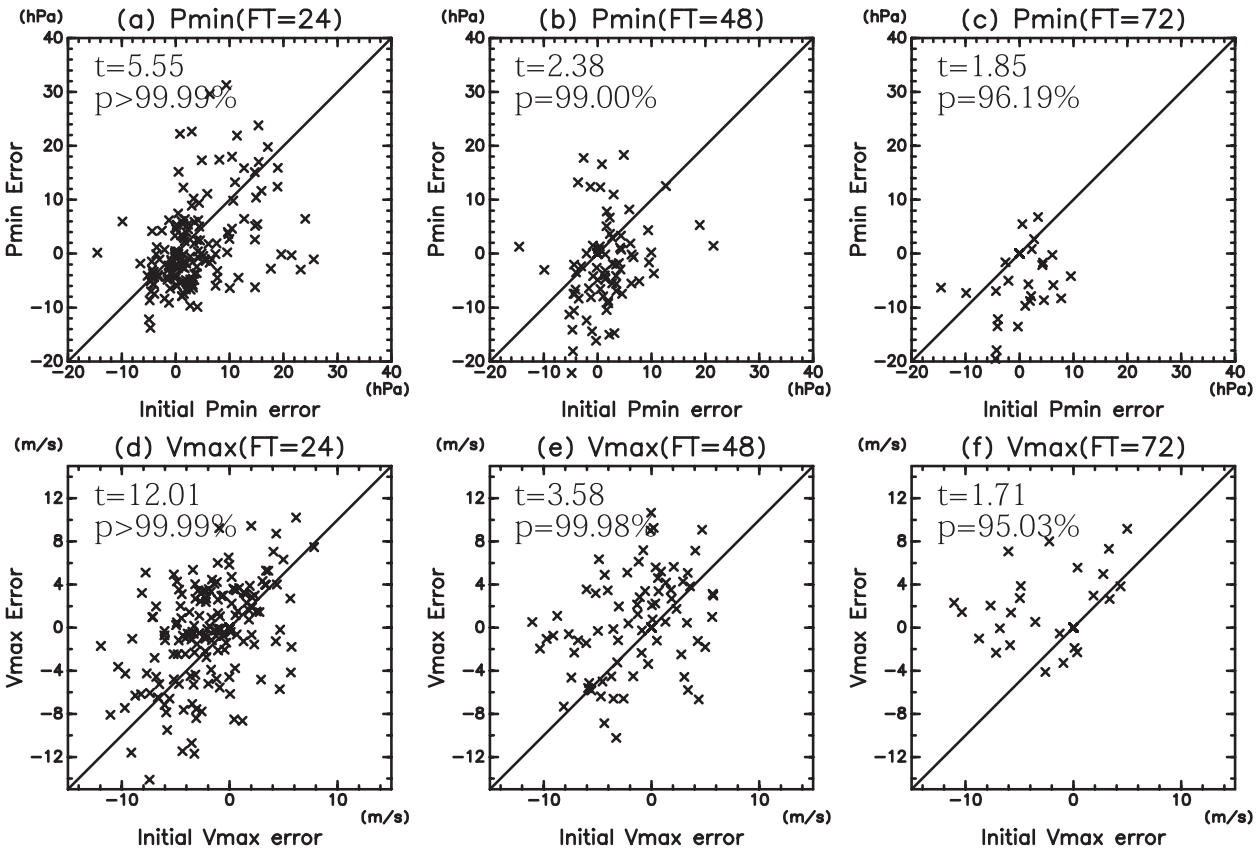

FIG. 13. Scatter diagram of the initial P_{min} errors and corresponding P_{min} errors at FT = (a) 24, (b) 48, and (c) 72 h in CMSM. (d)–(f) As in (a)–(c), but for the initial V_{max} error and the corresponding V_{max} errors.

higher than the observed values, particularly with increasing FT.

RMSEs of both P_{min} and V_{max} are the smallest in CMSM during most of the forecast period. The difference in P_{min} between AMSM and CMSM is noticeable at FT = 36 h and later. The improvement rates in CMSM relative to GSM and AMSM generally increase with increasing FT. The CMSM results are better than GSM and AMSM by about 27% and 21% at FT = 48 h in terms of minimum sea level pressure, respectively. Regarding maximum wind speed, CMSM is better than GSM and AMSM by about 13% and 20% at FT = 48 h, respectively. RMSEs in AMSM steadily increase with increasing forecast time, while in CMSM they tend to saturate beyond FT = 30 h.

TC intensities in GSM at the initial time have a low correlation with the best track and are negatively biased. When increasing the forecast time, the noncoupled models (AMSM and GSM) overintensify the TCs even with coarser grid spacing. CMSM shows the best forecast skill because the strong TCs at the initial time are better reproduced in the high-resolution model, and overintensification is suppressed along with sea surface cooling. The comparison between GSM and CMSM can result from differences in the physical schemes and parameter values other than the initial conditions and ocean coupling. Therefore, it is not easy to ascribe different results to individual factors. Nevertheless, this study reveals that a high-resolution atmosphere–ocean coupled model outperforms the TC intensity skill of the current state-of-the-art global model that is used for the operational TC intensity guidance.

In contrast, ocean coupling does not contribute to improving the TC track forecast, at least within the current framework of the experiments, while ocean coupling slightly deflects the TC position to the left of the storm motion on average. Further analysis shows that the initial error in TC intensity can persist for a long time and that the forecast skill of V_{max} is not very sensitive to the horizontal gridbox size used for defining the maximum wind speed.

There are limitations arising from the simplified ocean dynamics and assumptions considered in this study. For example, warm ocean eddies that contribute to rapid TC intensification (Lin et al. 2005, 2008; Ito et al. 2011) are not fully incorporated into this study because the subsurface

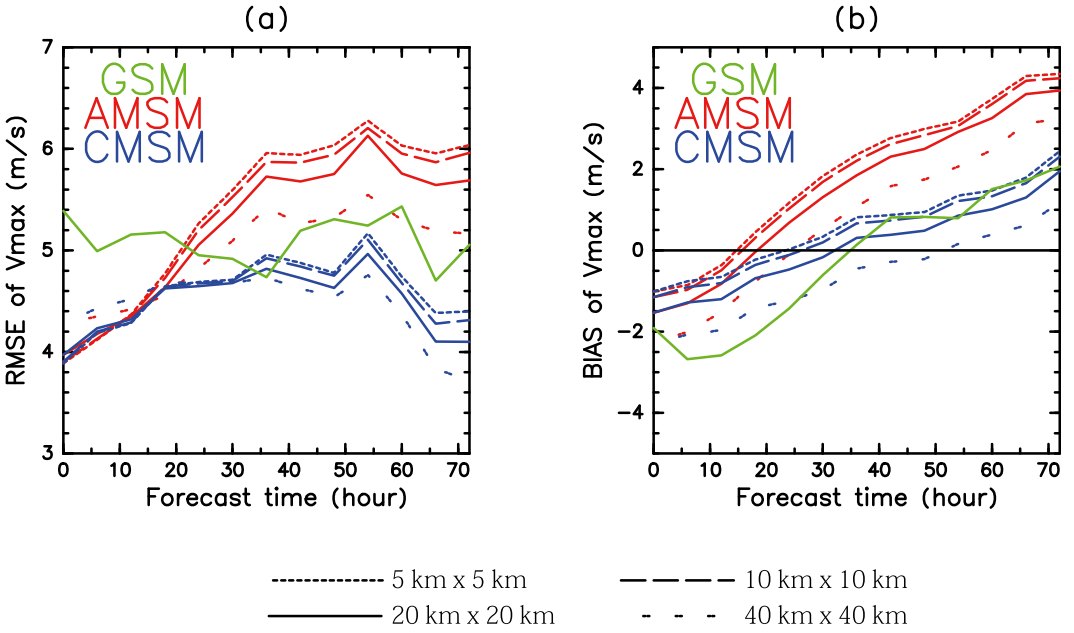

FIG. 14. As in Figs. 7 and 8, but for V_{max} by varying gridbox sizes: 1 × 1, 2 × 2, 4 × 4, and 8 × 8. The thicker line corresponds to the large gridbox size.

water temperature is set to climatology. Coupling a wave model to the atmospheric model may yield more realistic surface roughness lengths, which are currently parameterized using a bulk formula. Furthermore, most of the TCs analyzed in this study are in a decay stage and care should be taken when applying this method to developing TCs. The initial TC intensity error is thought to be another important source of forecast error. It requires a sophisticated data assimilation system and an improved bogussing approach. Better choices of the physical parameterization scheme and values of air–sea exchange coefficients are also important factors in terms of TC intensity forecasting. These factors can contribute to reproducing a TC vortex that has a more realistic thermodynamic and dynamic structure, and the role of these features remains for future works.

Nevertheless, the set of numerical experiments shown in this study is still meaningful. The large number of forecasts strongly confirms that the coupled high-resolution model reproduces a very realistic SST and therefore enhances the TC intensity forecast skill in comparison to noncoupled models. This leads to useful applications in the field of disaster prevention and mitigation.

Acknowledgments. We thank Drs. Y. Sato, S. Ishizaki, Y. Honda, T. Tsuyuki, H. Seko, F. Kimura, and T. Tokioka for providing useful comments. This work was supported by the Ministry of Education, Culture, Sports, Science, and Technology (MEXT) through the Strategic Programs for Innovative Research (SPIRE). AW was supported by MEXT KAKENHI Grant 25106708. All of the results were obtained using the K computer at the RIKEN Advanced Institute for Computational Science (Proposals hp120282, hp130012, and hp140220).

REFERENCES

Antonov, J., and Coauthors, 2010: *Salinity.* Vol. 2, *World Ocean Atlas 2009,* NOAA Atlas NESDIS 69, 184 pp.

Beljaars, A., and A. Holtslag, 1991: Flux parameterization over land surfaces for atmospheric models. *J. Appl. Meteor.,* **30,** 327–341, doi:10.1175/1520-0450(1991)030<0327:FPOLSF>2.0.CO;2.

Bender, M., I. Ginis, R. Tuleya, B. Thomas, and T. Marchok, 2007: The operational GFDL coupled hurricane–ocean prediction system and a summary of its performance. *Mon. Wea. Rev.,* **135,** 3965–3989, doi:10.1175/2007MWR2032.1.

Bryan, G., and R. Rotunno, 2009b: The maximum intensity of tropical cyclones in axisymmetric numerical model simulations. *Mon. Wea. Rev.,* **137,** 1770–1789, doi:10.1175/2008MWR2709.1.

Davis, C., and Coauthors, 2008: Prediction of landfalling hurricanes with the Advanced Hurricane WRF Model. *Mon. Wea. Rev.,* **136,** 1990–2005, doi:10.1175/2007MWR2085.1.

Emanuel, K., C. DesAutels, C. Holloway, and R. Korty, 2004: Environmental control of tropical cyclone intensity. *J. Atmos. Sci.,* **61,** 843–858, doi:10.1175/1520-0469(2004)061<0843:ECOTCI>2.0.CO;2.

Franklin, J., M. Black, and K. Valde, 2003: GPS dropwindsonde wind profiles in hurricanes and their operational implications. *Wea. Forecasting,* **18,** 32–44, doi:10.1175/1520-0434(2003)018<0032:GDWPIH>2.0.CO;2.

Ginis, I., and G. Sutyrin, 1995: Hurricane-generated depth-averaged currents and sea surface elevation. *J. Phys. Oceanogr.,* **25,** 1218–1242, doi:10.1175/1520-0485(1995)025<1218:HGDACA>2.0.CO;2.

Honda, Y., and K. Sawada, 2009: Upgrade of the operational mesoscale 4D-Var at the Japan Meteorological Agency. *Research Activities in Atmospheric and Oceanic Modelling,* CAS/JSC WGNE, 01.11–01.12. [Available online at http://www.wcrp-climate.org/WGNE/BlueBook/2009/individual-articles/01_Honda_Yuki_jnova.pdf.]

Ikawa, M., and K. Saito, 1991: Description of a non-hydrostatic model developed at the Forecast Research Department of the MRI. MRI Tech. Rep. 28, 238 pp. [Available online at http://www.mri-jma.go.jp/Publish/Technical/DATA/VOL_28/28_en.html.]

Ito, K., Y. Ishikawa, and T. Awaji, 2010: Specifying air–sea exchange coefficients in the high-wind regime of a mature tropical cyclone by an adjoint data assimilation method. *SOLA,* **6,** 13–16, doi:10.2151/sola.2010-004.

——, ——, Y. Miyamoto, and T. Awaji, 2011: Short-time-scale processes in a mature hurricane as a response to sea surface fluctuations. *J. Atmos. Sci.,* **68,** 2250–2272, doi:10.1175/JAS-D-10-05022.1.

——, T. Kawabata, T. Kato, Y. Honda, Y. Ishikawa, and T. Awaji, 2013: Simultaneous optimization of air–sea exchange coefficients and initial conditions near a tropical cyclone using jnova. *J. Meteor. Soc. Japan,* **91,** 337–353, doi:10.2151/jmsj.2013-307.

Jacob, S., L. Shay, A. Mariano, and P. Black, 2000: The 3D oceanic mixed layer response to Hurricane Gilbert. *J. Phys. Oceanogr.,* **30,** 1407–1429, doi:10.1175/1520-0485(2000)030<1407:TOMLRT>2.0.CO;2.

Japan Meteorological Agency, 2013: Annual report on the activities of the RSMC Tokyo-Typhoon Center 2012. Japan Meteorological Agency, 21 pp + appendixes. [Available online at http://www.jma.go.jp/jma/jma-eng/jma-center/rsmc-hp-pub-eg/AnnualReport/2012/Text/Text2012.pdf.]

——, cited 2014: Numerical weather prediction at the Japan Meteorological Agency. Japan Meteorological Agency. [Available online at http://www.jma.go.jp/jma/jma-eng/jma-center/nwp/nwp-top.htm.]

Kosaka, Y., and Y. Okagaki, 2010: Recent modifications of tropical cyclone bogus data in the JMA global data assimilation system. *Research Activities in Atmospheric and Oceanic Modelling,* CAS/JSC WGNE, 01.21–01.22. [Available online at http://www.wcrp-climate.org/WGNE/BlueBook/2010/individual-articles/01_kosaka_yuki_01_kosaka_yuki_TC_bogus.pdf.]

Kurihara, Y., T. Sakurai, and T. Kuragano, 2006: Global daily sea surface temperature analysis using data from satellite microwave radiometer, satellite infrared radiometer and in-situ observations (in Japanese). Weather Service Bull. 73, Japan Meteorological Agency, 1–18.

Lin, I., C. Wu, K. Emanuel, I. Lee, C. Wu, and I. Pun, 2005: The interaction of Supertyphoon Maemi (2003) with a warm ocean eddy. *Mon. Wea. Rev.,* **133,** 2635–2649, doi:10.1175/MWR3005.1.

——, ——, I. Pun, and D. Ko, 2008: Upper-ocean thermal structure and the western North Pacific category 5 typhoons. Part I: Ocean features and the category 5 typhoons' intensification. *Mon. Wea. Rev.,* **136,** 3288–3306, doi:10.1175/2008MWR2277.1.

Lloyd, I. D., and G. A. Vecchi, 2011: Observational evidence for oceanic controls on hurricane intensity. *J. Climate,* **24,** 1138–1153, doi:10.1175/2010JCLI3763.1.

Locarnini, R., A. V. Mishonov, J. I. Antonov, T. P. Boyer, H. E. Garcia, O. K. Baranova, M. M. Zweng, and D. R. Johnson, 2010: *Temperature.* Vol. 1, *World Ocean Atlas 2009,* NOAA Atlas NESDIS 68, 184 pp.

Manganello, J. V., and Coauthors, 2012: Tropical cyclone climatology in a 10-km global atmospheric GCM: Toward weather-resolving climate modeling. *J. Climate,* **25,** 3867–3893, doi:10.1175/JCLI-D-11-00346.1.

Nakanishi, M., and H. Niino, 2004: An improved Mellor–Yamada level-3 model with condensation physics: Its design and verification. *Bound.-Layer Meteor.,* **112,** 1–31, doi:10.1023/B:BOUN.0000020164.04146.98.

National Hurricane Center, cited 2013: National Hurricane Center Forecast verification. National Hurricane Center. [Available online at http://www.nhc.noaa.gov/verification/.]

Nishijima, K., T. Maruyama, and M. Graf, 2012: A preliminary impact assessment of typhoon wind risk of residential buildings in Japan under future climate change. *Hydrol. Res. Lett.,* **6,** 23–28, doi:10.3178/hrl.6.23.

Oouchi, K., J. Yoshimura, H. Yoshimura, R. Mizuta, S. Kusunoki, and A. Noda, 2006: Tropical cyclone climatology in a global-warming climate as simulated in a 20 km-mesh global atmospheric model: Frequency and wind intensity analyses. *J. Meteor. Soc. Japan,* **84,** 259–276, doi:10.2151/jmsj.84.259.

Price, J. F., 1981: Upper ocean response to a hurricane. *J. Phys. Oceanogr.,* **11,** 153–175, doi:10.1175/1520-0485(1981)011<0153:UORTAH>2.0.CO;2.

——, 1983: Internal wave wake of a moving storm. I: Scales, energy budget and observations. *J. Phys. Oceanogr.,* **13,** 949–965, doi:10.1175/1520-0485(1983)013<0949:IWWOAM>2.0.CO;2.

——, R. A. Weller, and R. Pinkel, 1986: Diurnal cycling: Observations and models of the upper ocean response to diurnal heating, cooling, and wind mixing. *J. Geophys. Res.,* **91,** 8411–8427, doi:10.1029/JC091iC07p08411.

——, T. Sanford, and G. Forristall, 1994: Forced stage response to a moving hurricane. *J. Phys. Oceanogr.,* **24,** 233–260, doi:10.1175/1520-0485(1994)024<0233:FSRTAM>2.0.CO;2.

Saito, K., 2012: JMA nonhydrostatic model and its applications to operation and research. *Atmospheric Model Applications,* I. Yucel, Ed., InTech, 85–110, doi:10.5772/35368.

——, and Coauthors, 2006: The operational JMA nonhydrostatic mesoscale model. *Mon. Wea. Rev.,* **134,** 1266–1298, doi:10.1175/MWR3120.1.

Sakai, R., and M. Yamaguchi, 2005: The WGNE intercomparison of tropical cyclone track forecasts by operational global models. *Research Activities in Atmospheric and Oceanic Modeling,* CAS/JSC WGNE, 2.7–2.8. [Available online at http://www.wcrp-climate.org/WGNE/BlueBook/2009/individual-articles/02_Onoda_Hirokatsu_02_onoda_hirokatsu_TCverification.pdf.]

Shay, L. K., 2010: Air–sea interactions in tropical cyclones. *Global Perspect. Trop. Cyclones,* **4,** 93–131, doi:10.1142/9789814293488_0003.

Wada, A., 2007: Numerical problems associated with tropical cyclone intensity prediction using a sophisticated coupled typhoon–ocean model. *Pap. Meteor. Geophys.,* **58,** 103–126, doi:10.2467/mripapers.58.103.

——, N. Kohno, and Y. Kawai, 2010: Impact of wave–ocean interaction on Typhoon Hai-Tang in 2005. *SOLA,* **6A,** 13–16, doi:10.2151/sola.6A-004.

——, N. Usui, and M. Kunii, 2013: Interactions between Typhoon Choi-wan (2009) and the Kuroshio Extension system. *Adv. Meteor.,* **2013,** 859810, doi:10.1155/2013/859810.

Walsh, K., M. Fiorino, C. Landsea, and K. McInnes, 2007: Objectively determined resolution-dependent threshold criteria for the detection of tropical cyclones in climate models and reanalyses. *J. Climate,* **20,** 2307–2314, doi:10.1175/JCLI4074.1.

Wang, Y., and C. Wu, 2004: Current understanding of tropical cyclone structure and intensity changes–a review. *Meteor. Atmos. Phys.,* **87,** 257–278, doi:10.1007/s00703-003-0055-6.

Yablonsky, R., and I. Ginis, 2009: Limitation of one-dimensional ocean models for coupled hurricane–ocean model forecasts. *Mon. Wea. Rev.,* **137,** 4410–4419, doi:10.1175/2009MWR2863.1.

Yau, M., Y. Liu, D. Zhang, and Y. Chen, 2004: A multiscale numerical study of Hurricane Andrew (1992). Part VI: Small-scale inner-core structures and wind streaks. *Mon. Wea. Rev.,* **132,** 1410–1433, doi:10.1175/1520-0493(2004)132<1410:AMNSOH>2.0.CO;2.

Yu, H., P. Chen, Q. Li, and B. Tang, 2013: Current capability of operational numerical models in predicting tropical cyclone intensity in the western North Pacific. *Wea. Forecasting,* **28,** 353–367, doi:10.1175/WAF-D-11-00100.1.